The *NFATc2* Gene Is Involved in a Novel Cloned Translocation in a Ewing Sarcoma Variant That Couples Its Function in Immunology to Oncology

Károly Szuhai,[1] Marije IJszenga,[1] Danielle de Jong,[1] Apollon Karseladze,[3] Hans J. Tanke,[1] and Pancras C.W. Hogendoorn[2]

Abstract

Purpose: Ewing sarcoma is an aggressive sarcoma and is the second most common bone sarcoma in childhood. Disease-specific t(11;22) (~85-90%), t(21;22) (~5-10%), or rarer variant translocations with the involvement of chromosome 22 (~5%) are present. At the gene level, the *EWSR1* gene fuses with *FLI1*, *ERG*, or other ETS transcription factor family members. Thus far, no Ewing sarcoma has been identified with a fusion to transcription factors other than ETS.

Experimental Design: Using molecular tools such as multicolor fluorescence *in situ* hybridization and array comparative genomic hybridization, a ring chromosome containing chromosomes 20 and 22 was identified in four Ewing sarcoma cases. The breakpoint was mapped with (fiber-) fluorescence *in situ* hybridization and reverse transcription-PCR followed by sequencing of the fusion partners.

Results: Molecular karyotyping showed the translocation and amplification of regions of chromosomes 20q13 and 22q12. Cloning of the breakpoint showed an in-frame fusion between the *EWSR1* and *NFATc2* genes, resulting in loss of the NH_2-terminal, calcineurin-dependent control region and an intact active domain of NFATc2 controlled by the transactivation domains of EWSR1.

Conclusion: A new translocation involving *EWSRI* and *NFATc2* was cloned. NFATc2 is a transcription factor that is not a member of the ETS family and functions in T-cell differentiation and immune response. Direct involvement of NFATc2 has not yet been observed in oncogenesis. We show that due to the shared sequence recognition of NFATc2 and the ETS family, shared transcriptional control is possible using activating protein complex 1.

Ewing sarcoma is an aggressive round cell sarcoma with various degrees of neuro-ectodermal differentiation. This tumor type is relatively uncommon, as it accounts for ~6% to 8% of primary malignant bone tumors, with a peak incidence below the age of 20 years. The occurrence of these tumors above the age of 30 years, or in people of African descent is very rare (1).

Ewing sarcoma is a model example of solid tumor formation mediated by a specific family of fusion genes. A balanced translocation occurs in the majority of cases between chromosomes 11 and 22, whereas variant rearrangements involving other chromosomes occur less frequently. Mapping of the breakpoint regions has led to the identification of specific chimera genes formed between *EWSR1* and various fusion partners such as *FLI1* (93%), *ERG* (5%), *ETV1*, *E1AF*, *FEV*, and *ZSG* (in the remaining cases), all members of the ETS transcription family (1, 2). The *EWS* gene acts here as a promiscuous gene and is found to be involved as a translocation partner in a range of other solid tumor types with a widespread histologic appearance (myxoid chondrosarcoma, angiomatoid fibrous histiocytoma, clear cell sarcoma, desmoplastic small round cell tumor; refs. 1–3, 4), or even in epithelial neoplasms (5). Importantly, none of these different histologic entities involves ETS gene family members as translocation partners, indicating the importance of the partner gene involved. The *EWSR1* gene may serve as a general translocation acceptor as the result of a genomic predisposition for translocation, caused in part by either active transcription (a housekeeping gene–like function) and/or the existence of sequence motifs predisposing the gene to nonallelic homologous recombination (6).

Detection of these rearrangements either by fluorescence *in situ* hybridization (FISH) or reverse transcription-PCR (RT-PCR)–based assays has had a great impact on the diagnosis of bone- and soft-tissue tumors. Specifically in the case of Ewing sarcoma, detection has helped in distinguishing tumors from other types in the group of small blue round cell tumors, especially those with an atypical clinicopathologic presentation.

The translocation leads to the replacement of the segment of the *EWSR1* gene that encodes an RNA binding domain with

Authors' Affiliations: Departments of [1]Molecular Cell Biology and [2]Pathology, Leiden University Medical Center, Leiden, the Netherlands, and [3]N.N. Blokhin Cancer Research Center, Moscow, Russia

Received 8/21/08; revised 12/22/08; accepted 1/14/09; published OnlineFirst 3/24/09.

The costs of publication of this article were defrayed in part by the payment of page charges. This article must therefore be hereby marked *advertisement* in accordance with 18 U.S.C. Section 1734 solely to indicate this fact.

Requests for reprints: Pancras C.W. Hogendoorn, Department of Pathology, Leiden University Medical Center, P.O. Box 9600, L1Q, 2300 RC Leiden, the Netherlands. Phone: 31-71-5266639; Fax: 31-71-5248158; E-mail: p.c.w.hogendoorn@lumc.nl.

doi:10.1158/1078-0432.CCR-08-2184

Translational Relevance

Ewing sarcoma is an aggressive childhood tumor. It is characterized by a fusion between the *EWSR1* gene and a member of the ETS transcription factor family mediated by a balanced translocation. Here, we report the identification and cloning of a novel translocation involving the *NFATc2* gene in a variant of Ewing sarcoma. NFATc2 has a described key role in both immune response and neuronal development and also plays a role in the inducible expression of cytokine genes in T cells. We show for the first time involvement of the transcription of NFATc2 as a fusion gene in solid tumor development, which has both clinical diagnostic and mechanistic implications. The *NFATc2* gene resides in the critical minimal region of genome amplification in several solid tumors such as breast, colon, and esophageal cancer, and the involvement of this transcription factor as a driver in the development of these tumors could thus be anticipated.

the DNA binding domain of an FLI-1 or ETS gene family member. The transcription of the formed "in-frame" chimera is driven by promoter-specific transactivation of EWSR1 (2, 6). At the protein level, this exchange results in transcriptional activation of several downstream genes controlled by members of the ETS transcription factor family. EWSR1 itself is a ubiquitously expressed gene with yet unknown functions, for which pseudogene sequences have been described (7). The chimera protein, using the DNA binding domain of the ETS family members (FLI1, ERG), forms a complex through activating protein complex 1 (AP1; FOS, JUN) transcription factor dimer, adding extra specificity for possible sequence recognition sites (8–10). Identification of these potential downstream target genes might shed light on the tumor biology of Ewing sarcoma, although only a limited number of downstream target genes has been identified in model systems (11, 12).

In this study, we describe in multiple cases the identification and molecular characterization of a novel translocation involving a member of the NFAT transcription factor family that results in a novel histologic variant of EWS. By using a panel of molecular techniques, we prove the existence of chimera formation between the *EWSR1* and *NFATc2* genes. The role of NFATc2 has been intensively studied in immune response, AIDS, and severe allergies, but no direct involvement of NFATc2 in tumor development has as yet been identified (13, 14).

We prove a direct oncogenic event of a chimeric gene formed by *EWSR1* and *NFATc2*, thereby showing the direct oncogenic involvement of the *NFATc2* gene in solid tumor formation.

Materials and Methods

Description of cases. A clinicopathologic overview of the cases is presented in Table 1.

Primary tumor culture and chromosome preparation. Collected tissue pieces were dissociated both mechanically and enzymatically. From short-term culture, chromosome preparations were made according to standard protocols, as described earlier (15).

Array comparative genomic hybridization. Array comparative genomic hybridization (array-CGH) tests were done according to standard protocols, as described earlier, using an in-house printed array-CGH containing ~3,700 large genomic insert clones (bacterial artificial chromosome, P1-derived artificial chromosome, cosmid, fosmid) distributed freely to academic institutions by the Welcome Trust Sanger Institute (group of Dr. N. Carter; refs. 15, 16).

Breakpoint mapping by FISH probes. Two cosmid probes covering the 5′ (G9) and 3′ (F7) parts of the EWS breakpoint regions in combination with probes on the 20q13 region were used to map the translocation breakpoint. The list of probes and their genomic location is given in Table 3. Labeling and hybridization of probes were done as described earlier (15, 17).

Table 1. Clinicopathological details of cases identified in this study

	L1231	L1857	MO1	MO2
Age	39	16	21	25
Gender	Male	Male	Male	Male
Localization	Right humerus	Right femur	Right thigh	Right femur
Immunostaining				
CD99	Membranous pos	Membranous pos	Scattered, membranous pos	Membranous pos
Vimentin	Pos	Pos	Pos	Pos
BCL2	Pos	Pos	Pos	NT
CD3	Negative tumor cells/scattered infiltrating lymphocyte	Negative tumor cells/scattered infiltrating lymphocyte	Negative tumor cells/scattered infiltrating lymphocyte	NT
CD56	Neg	Neg	Neg	NT
Desmin	Neg	Neg	Neg	Neg
CD117	Neg	Neg	NT	NT
CD45	Neg	Neg	NT	NT
CD56	Neg	Neg	NT	NT
CD57	Neg	Neg	NT	NT
CD68	Neg	Neg	NT	NT
Keratin	Neg	Neg	Neg	Neg
NSE	Neg	Neg	Neg	Neg
S100	Neg	Neg	Neg	Neg

Abbreviations: Pos, positive; Neg, negative; NT, not tested.

Table 2. Primer sequences used

Primer name	Position	Sequence (5′-3′)	Gene name	Accession no.
NFATc2_1842_R	1842-1823	CGCGTGTTCTTTCTTCCAAT	*NFATc2*	NM_012340
NFATc2_867_F	867-886	CCTCGCCAATAATGTCACCT	*NFATc2*	NM_012340
NFATc2_3220_R	3220-3202	CGCTTAGTGCCCATACATT	*NFATc2*	NM_012340
EWSR1_731_F	762-783	TCAATCTAGCACAGGGGGTTAC	*EWSR1*	NM_005243
EWSR1_1561_R	1561-1542	CATAGGACACTGTGGCATCG	*EWSR1*	NM_005243
EWSR1_755_F	755-777	GTCAACCTCAATCTAGCACAGGG	*EWSR1*	NM_005243
EWSR1_271_F	271-290	GGAGACGGACGTTGAGAGAA	*EWSR1*	NM_005243
FLI1_1053_R	1053-1040	CTGTCGGAGAGCAGCTCCAG	*FLI1*	NM_002017
ERG_1064_R	1064-1044	CTGTCCGACAGGAGCTCCAG	*ERG*	NM_182918

NOTE: To detect the EWSR1-NFATc2 fusion transcript, the primers EWSR1_731_F and NFATc2_1842_R were used. To detect the NFATc2-EWSR1 fusion transcript, the primers NFATc2_867_F and EWSR1_1561_R were used. As controls to detect EWSR1-FLI1 or EWS-ERG fusion transcripts, EWSR1_755_F and FLI1_1053_R or EWSR1_755_F and ERG_1064_R were used, respectively. To detect the normal NFATc2 transcript, NFATc2_867_F and NFATc2_1842_R were used, and for the EWSR1 normal transcript, EWSR1_755_F and EWSR1_1561_R were used.

Preparation of DNA fibers for breakpoint mapping. To fine map the breakpoint region at the genomic level, cells from short-term primary tumor cultures of L-1231 were collected in suspension. Linearly extracted, stretched DNA fibers were made from cells using the so-called "halo technique," which has been described for high-resolution FISH mapping (18).

RNA isolation, reverse transcription reaction. Total RNA was extracted from snap-frozen tumor tissues of Ewing sarcoma patients L-1231, L-1857, and M01, and from the cell lines TC32, TTC-466, and EW3 (19) using the Trizol reagent (Life Technologies, Invitrogen) according to the manufacturer's recommendations. cDNA synthesis using 5 μg of total RNA was done with the SuperScript III first strand synthesis system for RT-PCR (Invitrogen) with oligo$(dT)_{20}$ primers in a final volume of 20 μL as described by the manufacturer.

Reverse transcription-PCR. RT-PCR for EWSR1-NFATc2, NFATc2-EWSR1, EWSR1-FLI1, and EWSR1-ERG was done. RT-PCR for NFATc2 and EWSR1 for the nontranslocated genes was also done. The Ewing sarcoma cell line cDNA TC32 was used as a positive control for EWSR1-FLI1 translocation; TTC446 and EW3 were used as positive controls for EWSR1-ERG translocation. All PCR amplifications were done in a 50 μL reaction volume containing 20 mmol/L Tris-HC1 (pH 8.0), 1.5 mmol/L $MgCl_2$, 0.2 mmol/L of each deoxynucleotide triphosphate, 2 units AmpliTaq polymerase (Applied Biosystems), 0.5 μmol/L of each of the forward and reverse primers, and 2 μL of 1:5 diluted synthesized cDNA. Primer positions were assigned according to reference sequences of NFATc2: NM_012340, EWSR1: NM_005243, FLI1: NM_002017, and ERG: NM_182918. Detailed information about the position, length, and direction of the primers used are reported in Table 2. Different primer combinations were used. To detect the EWSR1-NFATc2 fusion transcript, the primers EWSR1_731_F and NFATc2_1842_R were used. To detect the NFATc2-EWSR1 fusion transcript, the primers NFATc2_867_F and EWSR1_1561_R were used. As controls to detect EWSR1-FLI1 or EWS-ERG fusion transcripts, EWSR1_755_F and FLI1_1053_R or EWSR1_755_F and ERG_1064_R were used,

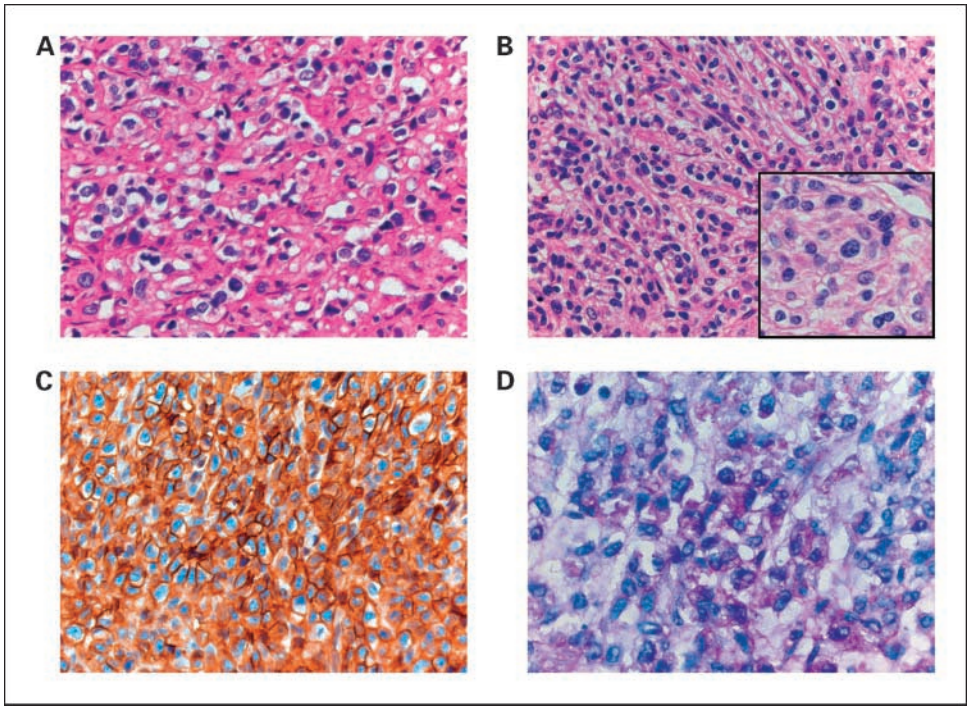

Fig. 1. Histomorphologic and immunophenotypic features. Light micrographs showing tumor cells with rounded occasionally somewhat buckled nuclei (*A*, case M01; *B*, case L1231). The tumor cells grow diffusely, although sometimes in a nest-like pattern surrounded by slight sclerosis (*A*). Scattered cells with a somewhat bigger nucleus are found with a prominent nucleolus, cells with buckled nuclei (*inset* in *B*). There is strong, diffuse, membranous staining for CD99 (*C*). Note the presence of clear, somewhat granular cytoplasm, which is strongly periodic acid-Schiff positive (*D*).

respectively. To detect the normal NFATc2 transcript, NFATc2_867_F and NFATc2_1842_R were used, and for the EWSR1 normal transcript, EWSR1_755_F and EWSR1_1561_R were used.

All PCR reactions consisted of an initial denaturation step of 4 min followed by 35 cycles of denaturation at 94°C for 30 s, annealing at 60°C for 30 s and elongation at 72°C for 1 min, and then a final extension of 10 min at 72°C. Ten microliters of the PCR products were analyzed by electrophoresis with 1.5% agarose gels stained with ethidium bromide and photographed.

To amplify the full-length fusion product, the Expand Long Template PCR system (Roche Applied Science) was used in a 50 μL reaction volume containing Expand long template buffer 1, 0.2 mmol/L of each deoxynucleotide triphosphate, 3.75 units of Expand long template mix, 0.5 μmol/L of the primers NFATC2-3220-R and EWSR1_271_F, and 1 μL of 1:5 diluted synthesized cDNA. Thermal cycling conditions were initial denaturation at 94°C for 2 min, 35 cycles consisting of denaturation at 94°C for 10 s, annealing at 62°C for 30 s and elongation at 68°C for 3 min, followed by a final extension step at

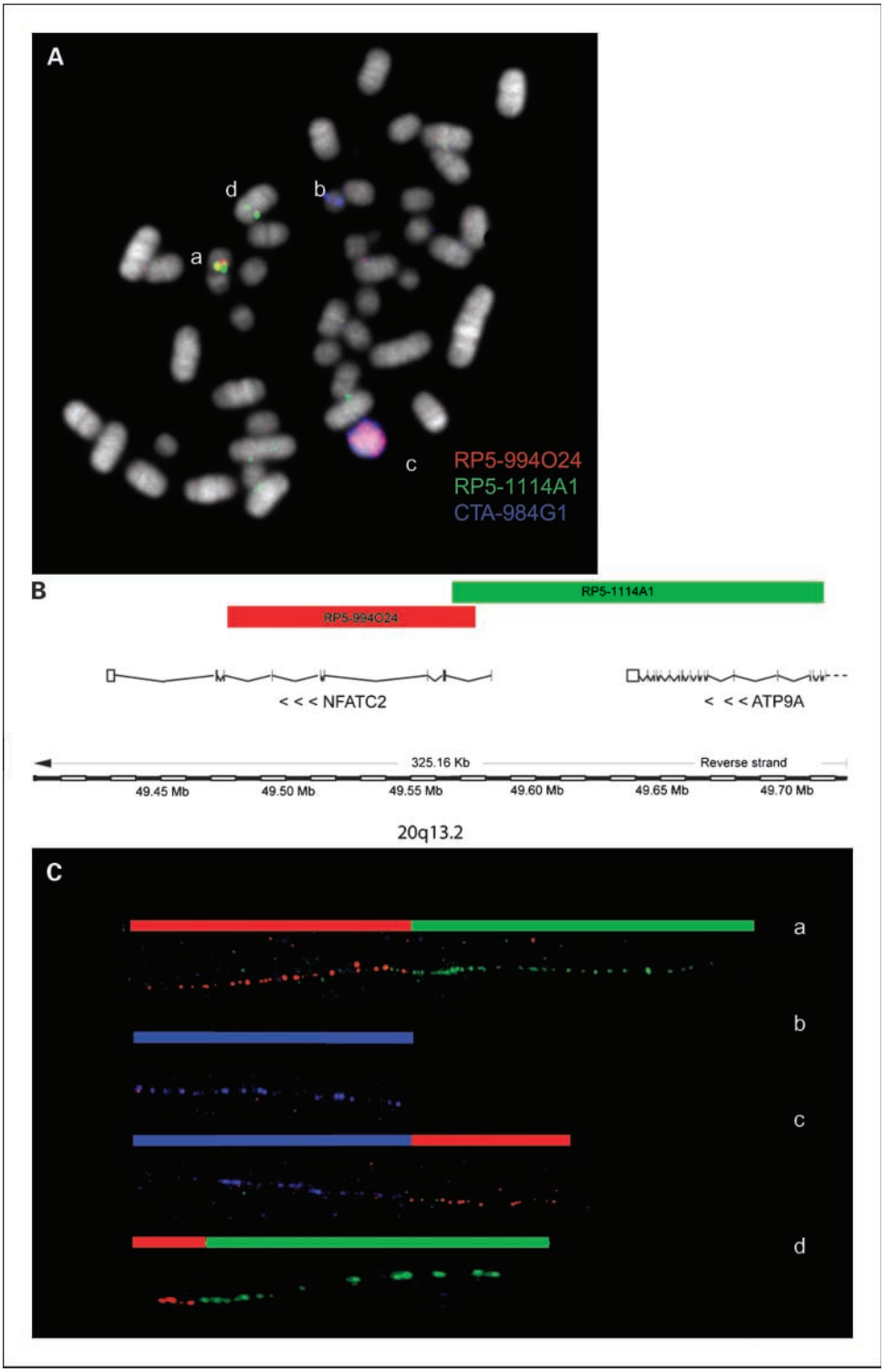

Fig. 2. FISH mapping of the translocation breakpoints. *A,* using a set of bacterial artificial chromosome probes located on chromosome 22 (CTA-984G1, *blue*) proximal to the breakpoint and two probes on chromosome 20 (RP5-994O24, *red*; RP5-1114A1, *green*) bracketing the breakpoint on chromosome 20, a split of the latter probes and a fusion of the RP5-994O24 and the CTA-984G1 were observed. *B,* mapping of bacterial artificial chromosome clones RP5-994O24 and RP5-1114A1 in relation to the NFATc2 genomic region on chromosome 20q13. *C,* representative fiber-FISH images. Using the same color combination for the probes as for breakpoint mapping in Fig. 1A, all rearrangements were confirmed and the NFATc2 breakpoint was further mapped. The letters in both figures indicate the normal chromosome 20 (*a*), normal chromosome 22 (*b*), the ring chromosome 20;22 (*c*), and the derivative chromosome 14 with retained regions of chromosome 20 (*d*).

Table 3. Overview of genomic alterations detected by array-CGH

Alteration	L1231*	L1857	M-01
Loss			
9q22.33-q32.2	RP11-66O2 > > RP11-30L4 (~20.6 Mb) RP11-23J9 > > RP11-417B4 (~27.9Mb)	RP11-141J10 > > RP11-143H20 (~60.3 Mb)	None
10 pter-p14	GS-23B11 > > RP11-730A19 (~11.8 Mb)	None	None
20pter-p11.1	GS-1061L1 > > RP11-348I14 (~28.2 Mb)	RP11-314N13 > > RP11-504H3 (~18.1 Mb)	RP4-741H3 > > RP11-504H3 (~13.4 Mb)
20q11-12	RP5-1161H23 > > RP11-122O1 (~4.7 Mb) RP1-138B7 > > RP5-1028D15 (~1.8 Mb)	None	None
Gain			
20p	None	None	RP5-1096J16 > > RP5-1025A1 (~5.1Mb)
20q	RP3-324O17 > > RP5-914B9 (~3.1 Mb) RP4-600E6 > > RP1-232N11 (3.1 Mb) RP4-781B1 > > RP5-994O24 (~7.3 Mb)	RP3-324O17 > > RP5-994O24 (~20.1 Mb)	RP3-324O17 > > RP5-994O24 (~20.1 Mb)
22q	RP11-155F20 > > CTA57G9 (~8.5 Mb)	RP11-155F20 > > CTA57G9 (~8.5 Mb)	RP11-155F20 > > CTA57G9 (~8.5 Mb)

*Array-CGH results of this case have been described in ref. (18).

68°C for 7 min. Ten microliters of the PCR product were analyzed by electrophoresis on 0.8% agarose gels stained with ethidium bromide and photographed.

For sequence analysis, the amplified cDNA fragments were purified from the gel, using the Qiagen gel extraction kit (Qiagen), and directly sequenced using an ABI Prism BigDye terminator cycle sequencing ready reaction kit (PE Applied Biosystems) on the Applied Biosystems Model 373A DNA sequencing system.

Cloning. The PCR-amplified sequences of the complete chimera genes L-1231 and L-1857 were cloned into the pGEM-TEasy vector system (Promega) according to the manufacturer's recommendations. Recombinant plasmid DNA was isolated with the High Pure plasmid isolation kit according to the manufacturer's recommendations (Roche Applied Sciences).

All isolated plasmids containing the PCR product were sequenced as described above using standard M13 sequencing primers.

Interphase FISH. For case M02, interphase FISH on 6-μm-thick paraffin sections was done as described earlier (3). Two sets of FISH probes were labeled using a standard nick translation reaction as described earlier (17). Set 1, containing the RP5-994O24 and RP5-1114A1 bacterial artificial choromosome clones covering the NFATc2 genomic region, was used as a "split apart" probe set to show the rearrangement of the 20q region. Set 2, containing RP5-994O24 on chromosome 20 and CTA-984G1 on chromosome 22, was used as a colocalization probe set.

Results

Histology. Microscopically, the tumor consisted of a compact proliferation of tumor cells admixtured with scattered cells that had moderately pleiomorphic rounded nuclei with coarse chromatin and a prominent nucleolus (Fig. 1). The cytoplasm showed a granular appearance and was periodic acid-Schiff positive and not diastase resistant. Areas of necrosis were observed, and there was infiltration and destruction of the surrounding bone. Scattered numerous mitoses were found. The tumor cells were sometimes arrayed in a nest-like pattern with slight peritumoral fibrosis. Immunohistochemically, there was expression of vimentin CD99 (Fig. 1) and BCL-2, whereas desmin, CD45, CD57, CD56, CD3, CD68, CD117, and S-100 were negative. The strong CD99 and vimentin staining and the absence of staining for a panel of other markers used in the differential diagnosis of small round cell sarcomas supported the diagnosis of EWS despite the presence of atypical cellular features.

Array-CGH, FISH mapping and fiber-FISH, interphase FISH. Based on the array profile, bacterial artificial chromosome clones covering the borders of the 20q amplified regions were selected and tested for FISH. By using this approach, FISH mapping toward the transition of the breakpoint region was done by using pair-wise labeled probes on metaphase chromosomes of case L1231. By using the bacterial artificial chromosome probes RP5-994O24 (proximal, *red*) and RP5-1114A1 (distal, *blue*) localized on chromosome 20, a split signal was observed in the proximal probe. The signals were observed both in the ring marker chromosome colocalizing with the *EWSR1* gene region–specific probe (CTA-984G1, *green*) and in the derivative chromosome 14 containing the distal part of chromosome 20q (Fig. 2A). Finally, fine mapping of the breakpoint region was done using the fiber-FISH technique with the previously mentioned three probes. This technique allows for breakpoint mapping on stretched DNA with a resolution of ~5 to 10 kb. The resulting FISH image showed that the breakpoint was localized within the distal third of the RP5-994O24 probe (Fig. 2B and C). Based on the fiber-FISH results, the breakpoint was localized within the *NFATc2* gene at the 5′ region. The clone RP5-994O24 contains exon 1 and intron 1 of *NFATc2* and the distal gene region toward and including the *ATP9A* gene. The clone RP5-1114A1 is located proximal to RP5-994O24 and contains a smaller region of intron 1, full regions of exon 2 to exon 5 with intron 2 to 4, and a smaller region of intron 5. Based on the length of the fibers and the position of the breakpoint, the breakpoint was estimated to be in the region of intron 2 and intron 3 (Fig. 2B).

Because no viable cells were available from the additional two cases, array-CGH was done to investigate the genome composition. Array-CGH profiles of both cases showed a highly similar amplification pattern involving chromosomes 20 and

22. A secondary alteration, such as the deletion on the long arm of chromosome 9, was almost identical in cases L1857 and L1231, whereas alteration of chromosome 9 was not present in the M01 case. In addition, an overlapping 14.5-Mb deletion was observed on the long arm of chromosome 20 between q11.2 and q13.2, containing at least 300 genes. A detailed description of gains and losses detected in all three cases by array-CGH is shown in Table 3.

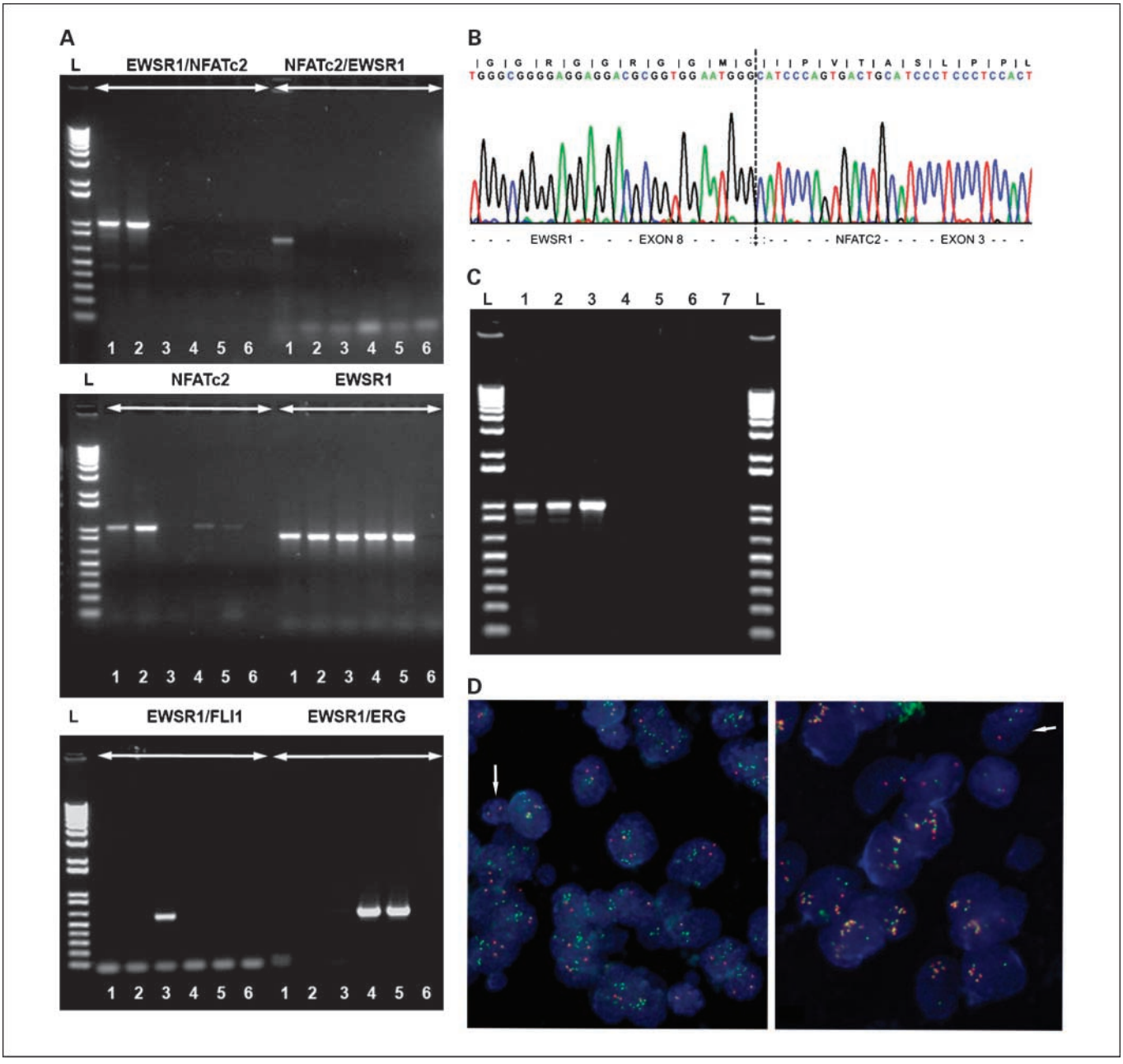

Fig. 3. RT-PCR and sequencing results. *A,* RT-PCR results by using a panel of primer sets to detect expression of EWSR1/NFATc2, NFATC2/EWSR1, NFATc2, EWSR1, EWSR1/FLI1, and EWSR1/ERG mRNA sequences (combinations are indicated on the top of each panel; primer sequences are given in Table 2). Samples used these tests: 1, L1231; 2, L1857; 3, TC32; 4, TTC-466; 5, EW3; 6, no template control. Gel document shows a specific amplicon of ~900 bp by using primers for the *EWSR1* and *NFATc2* genes for cases L1231 and L1857 (*top left*). The reciprocal fusion of NFATc2/EWSR1 was observed only for case L1231 (*top right*). For both primer combinations, no amplicon was seen for the control cell lines (TC32, TTC466, and EW3) and no template control samples. Both primary tumor samples and the two EWSR1/ERG fusion-containing cell lines showed expression of the NFATc2 RNA from the normal allele (*middle left*), whereas expression of the EWSR1 RNA was detected in all analyzed samples, except the no template control (*middle right*). Specific amplification of the EWSR1/FLI1 fusion was seen for the TC32 cell line (*bottom left*) and amplification of the EWSR1/ERG fusion product for the TTC466 and EW3 cell lines (*right bottom*). *B,* partial sequence chromatogram showing the junction of the EWSR1 and NFATc2 genes (*dashed line*). The fusion between exon 8 of EWSR1 and exon 3 of NFATc2 resulted in an in-frame transcript, as shown by the resulting amino acid sequence above the sequence readout. *C,* RT-PCR using a primer combination to detect the presence of the EWSR1/NFATc2 fusion product in the three samples with available frozen tissue. Samples used these tests: 1, L1231; 2, L1857; 3, M-01; 4, TC32; 5, TTC-466; 6, EW3; 7, no template control. *D,* interphase FISH using overview using two sets of FISH probes, case M-02. *Left,* set 1 RP5-994O24 and RP5-1114A1 BAC clones covering the NFATc2 genomic region were used as a "split apart" probe set to show the split and amplification of the green signal on chromosome 20q (*arrowhead,* normal cell with colocalizing signals). *Right,* set 2 consisting of RP5-994O24 on chromosome 20 and CTA-984G1 on chromosome 22 was used as a colocalization probe set. Colocalization and amplification of the EWSR1 and NFATc2 regions is visible (*arrowhead,* normal cell with separated signals).

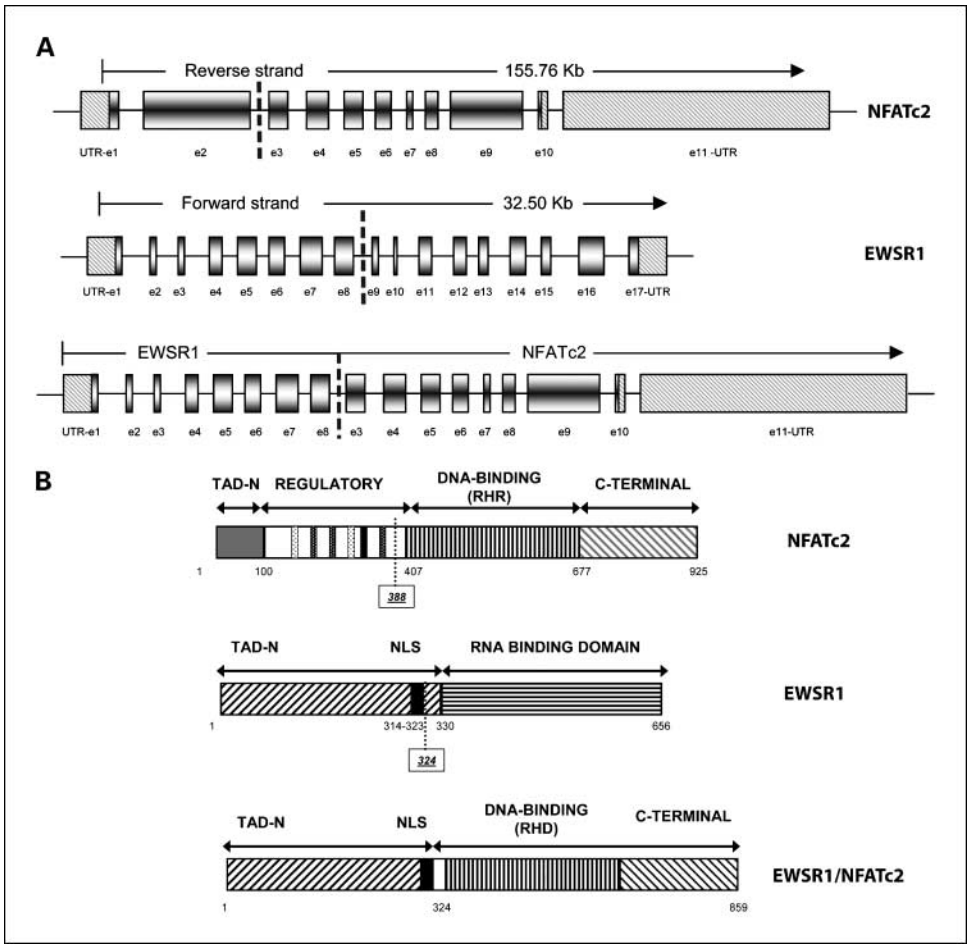

Fig. 4. Schematic representation of the translocation breakpoint and the resulting chimera protein. *A,* genomic organization of the *NFATc2* and *EWSR1* genes. Filled boxes, exons; dashed boxes, untranslated regions (*UTR*); connecting lines, intron regions. The lengths of the exon boxes are proportional to the actual sequence length, whereas the intron regions are not; the full genome coverage and strand orientation are indicated. Vertical dashed lines, the translocation breakpoints within intron 2-3 of *NFATc2* and intron 8 of *EWSR1*. The full-length fusion gene contains 17 exons. *B,* protein structure with indications of functional domains of NFATC2, EWSR1, and the fusion product. The translocation resulted in a loss of the NH_2-terminal control domain (*TAD-N*) and the regulatory domain of the NFATc2 protein containing multiple conserved phosphorylation sites. Solid black block, NLS; black and white dotted blocks, serine-rich regions (SRR1 and SRR2) and three SPxx repeat motifs, respectively. The EWSR1 protein is thought to act through a COOH-terminal RNA binding domain, and nuclear trafficking of the protein is signaled by a conserved NLS (*black box*). Vertical dashed lines, breakpoints in both protein sequences. The fusion protein contains the TAD-N of EWSR1 with its NLS and the functionally active RHD of NFATc2.

RT-PCR, sequencing, and cloning. Using fiber-FISH results, primers were designed for RT-PCR. A reverse primer located in exon 5 of the *NFATc2* gene and a forward primer located in exon 6 of the *EWSR1* gene were selected. Because in the normal genome, no such gene construct is transcribed, this primer combination was considered to be specific for the chimera cDNA sequences only. With the RT-PCR reaction, a PCR fragment of ~900 bp was obtained (Fig. 3A). Direct sequence analysis proved that the fragment was a hybrid cDNA containing sequences from EWSR1 (22q12.2) and NFATc2 (20q13). Detailed analysis of the sequence showed a junction between the 3′ end of exon 8 of EWSR1 and the 5′ end of NFATc2 exon 3, forming an in-frame transcript (Fig. 3B). Primers to amplify and clone a full-length chimera cDNA were designed, followed by cloning of the amplified product into a plasmid vector (Genbank accession: L1231: FJ573259, L1857: FJ573260, M-01: FJ573261). Further analysis of the chimera sequence revealed an in-frame sequence that could be translated to an 859-amino-acid protein sequence (Fig. 3B).

Purely based on their histologic appearance, three additional clinical cases were identified (L1857, M-01, and M-02). For case M-01, a limited frozen sample was available; for M-02, only FFPE material was available. RT-PCR was done on cases L1857 and M-01, whereas interphase FISH was done on M-02. By using RT-PCR, the presence of the very same translocation was detected in both cases, whereas no product was formed using the primer combination for the EWSR1/FLI1 or EWSR1/ERG chimera sequences. As controls, we used the cell lines TC32, containing EWSR1/FLI1, and TTC466 and EW3, containing EWSR1/ERG rearrangements. Expression of the wild-type EWSR1 was found in all samples and cell lines (Fig. 3A).

To investigate the presence of an expressed reciprocal gene product derived from the NFATc2/EWSR1 fusion, an additional RT-PCR reaction was done using the NFATc2_867_F and EWSR1_1561_R primer combination. An amplified product was observed only from case L1231, and not from the other two cases (Fig. 3A).

Sequence analysis. In all cases, an in-frame chimera was formed. Translation of the sequences to proteins resulted in chimera protein sequences containing the COOH-terminal region of EWSR1, coded by the first eight exons, and the NH_2-terminal region of NFATc2, coded by exons 3 to 10 (Fig. 3B and 4A).

The resulting fusion protein lacks the COOH-terminal RNA binding domain of EWSR1 and the NH_2-terminal transactivation domain and regulatory domain of NFATc2, containing both the conserved phosphorylation sites and nuclear localization signal (NLS; Fig. 4B). The region of the EWSR1 protein coded by exon 8 provides a strong, highly conserved NLS (amino acids 314-323) to the fusion with the RGGR-GGGRG sequence, allowing for nuclear localization of the fusion product without any retained control from the NFATc2 protein (Fig. 4B).

Interphase FISH. For case M-02, only FFPE samples were available for testing by interphase FISH. Two sets of FISH

probes were labeled to detect (*a*) the breakpoint within the *NFATc2* gene region as a split of the signal by using RP5-994O24 and RP5-1114A1 clones and (*b*) the presence of translocation between the proximal, amplified NFATc2 region and the proximal EWSR1 region using the RP5-994O24 and CTA-984G1 clones. A split of the signal using set 1 and colocalization of the signal using set 2 was observed (Fig. 3). Similarly, the other cases detected by array-CGH, amplification of the proximal EWSR1, and the proximal NFATc2 region were also observed.

Diagnostic relevance. By using RT-PCR reactions, we showed that the selected primer combination specifically detects the presence of the transcribed fusion product. Furthermore, we proved that the selected FISH probe set can be used as a reliable diagnostic tool to detect the presence of the translocation and amplification in interphase cells if only archived samples are available.

Discussion

In this study, we describe the identification and cloning of a novel translocation involving the *NFATc2* gene in a histologic variant of Ewing sarcoma. We show for the first time the involvement of NFATc2 in tumor development as a fusion gene. NFATc2 (MIM: 600490; nuclear factor of activated T-cells, cytoplasmic, calcineurin-dependent 2, also known as NFAT1 or NFATp) is a transcription factor that has a described key role both in immune response and in neuronal development (13, 14, 20). It also plays a role in the inducible expression of cytokine genes in T cells, especially in the induction of the interleukin 2, interleukin 3, interleukin 4, tumor necrosis factor-α, and granulocyte macrophage colony-stimulating factor (21, 22). Tumor immunologic aspects of Ewing sarcoma have recently attracted attention. Ewing sarcoma, particularly in the advanced stage, frequently shows a complete or partial absence of both classes of HLAs.[4] This may affect both immune surveillance and the efficacy of cellular immunotherapy. It was shown, however, that natural killer cells recognize and are able to lyse Ewing sarcoma cells via the NKG2D and DNAM-1 receptor pathways (23). It is thought that this interaction is promoted predominantly by activating signals in Ewing sarcoma cells. Interestingly, Ewing sarcoma cell lines express cFLIP but are resistant to CD95/Fas–mediated apoptosis when caspase-8 expression is lacking. In primary Ewing sarcomas, including metastases, cFLIP was abundantly expressed; however, caspase-8 showed more intertumoral and intratumoral variation (24). Whether NFATc2 or homologous acting gene fusions play a role in immunomodulation in Ewing sarcoma requires further study.

The function of the NFATc2 protein is controlled by Ca^{2+} signal-dependent activation by calcineurin. Dephosphorylation of the inactive, phosphorylated, cytoplasmic protein in turn results in nuclear translocation and functional activation of the protein. This activated NFATc2 protein forms a complex with AP1, a complex formed by the fos and jun proteins (13, 25). Both AP1 and NFATc2 are capable of recognizing a specific DNA sequence in promoter regions, which results in concerted regulation of gene expression. Notably, the ETS family of transcription factors, similarly to NFAT, forms a transcription complex with AP1 (8, 9).

NFATc2 is a transcription factor, a member of the NFAT protein family with a highly conserved DNA binding domain that is structurally related to the Rel family of transcription factors. The Rel homology region is characteristic of NFAT proteins (Fig. 4B), which show no similarity to the ETS transcription factor family, known to be involved in Ewing sarcoma.

In all cases, a fusion between exon 8 of EWS1 and exon 3 of NFATc2 in the chimera gene was identified (Figs. 3 and 4). At the genome level, the breakpoints were located in intron 8 on chromosome 22 and intron 2 on chromosome 20 in the *EWSR1* and *NFATc2* genes, respectively. At the protein level, the EWSR1 breakpoint resulted in the loss of the RNA binding domain region, similarly to other Ewing sarcoma–specific translocations. For the translocation partner NFATc2, loss of the first two exons resulted in truncation of the first 387 amino acids of the NH_2-terminal domain. This NH_2-terminal domain contains the control region of the NFATc2 protein, including the calcineurin binding region SPRIET and the activation domains SP-2, SP-3, and SRR-NLS, containing a NLS (Fig. 4). Inactive NFAT protein, also called preexisting component NFATp, is phosphorylated at these sites and localizes in the cytoplasm. Upon external stimuli, calcineurin-mediated dephosphorylation of NFAT results in configuration changes and exposes the NLS. In the nucleus, NFATc2 protein forms a complex through the Rel homology region (DNA binding domain) with the AP1 transcription complex and subsequently activates gene expression (20, 21). The identified chimera contains a full, intact RHR and a second (weaker) NLS in the COOH-terminal region; therefore, a constant activation of the transcription factor through the RHR is possible. In case of translocation, EWSR1 is thought to operate as a promoter-specific transactivator (6). The expression of the chimera gene is driven by the EWSR1 promoter, abrogating the self-regulatory loops of NFATc2. Interestingly, in this novel translocation, the SRR–NLS of NFATC2 has been replaced by a highly conserved NLS of the EWSR1 protein (RGGRGGGRG) located in exon 8 of the *EWSR1* gene, facilitating uncontrolled nuclear translocation of the fusion protein (Fig. 4B).

Because transcription factors are known to have high sequence specificity, resulting in restricted and recognizable tumor appearance, an Ewing sarcoma–like phenotype would not be expected. Furthermore, additional target sequence specificity is added both for ETS members and for NFAT by forming a complex AP1 (heterodimer of fos and jun proteins). This cooperative action has been well documented both for ETS-AP1 (8), ERG-AP1 (9), and more interestingly for EWSR1/FLI1-AP1 (10) and NFAT-AP1 (25). It has been shown that both NFAT and ETS transcription factors interact with the bZIP motifs of the Fos-Jun complex (9, 10, 25, 26). Intriguingly, when comparing the sequence recognition patterns of these two gene families (ETS and NFAT), an overlap of the core consensus sequence was observed. The consensus sequence for the ETS family contains a core domain of GGAW (W is a wobble for A or T), whereas the conserved core domain for NFAT is WGGAAANHN (H is not G, N is any of the four nucleotides). There is complete overlap between the core domain of ETS and NFAT for the GGAA sequence variant. Because both genes use

[4] Berghuis et al., J Pathol 2009. doi: 10.1002/path.2537.

the AP1 complex for higher specificity of target recognition, we have performed *in silico* target identification by using the CHIP MAPPER tool and database (27). By using EWSR1-FLI1 regulated genes described in the literature, such as ID2, MNFG, and PGDFC, we were able to identify sequence motifs shared both for ETS and NFAT binding in combination with AP1 sites, which supports the possibility of shared downstream regulation. Several ETS transcription factors could be coexpressed within the same tissue, showing that over half of the 27 paralogues of human *ets* genes are expressed ubiquitously (28). Remarkably, neither FLI1 nor ERG belongs to this group, indicating their higher tissue specificity.

This *in silico* test identified a potential NFATc2 binding site at the promoter region of all target genes of FLI1 and ERG in combination with the AP1 complex, which influences the expression of these transcription factors. Similarly to FLI1 and ERG, NFATc2 is not ubiquitously expressed. To investigate the influence of EWS/ETS (FLI1 or ERG) chimeras, we studied the expression of NFATc2 in EWS cell lines. The use of cell lines instead of biopsy samples would preclude the false-positive detection of NFATc2 expression derived from tumor infiltrating and/or circulating T cells and B cells and macrophages/mast cells. In the EWS/FLI1 containing cell line, no expression of NFATc2 was detected, whereas a low expression level was observed in both cell lines with the EWS/ERG translocation, which indicates a potential transcriptional cross-talk driven by the chimera sequence (EWSR1/ERG) in the promoter region of NFATc2.

From the clinical point of view, the fusion of the *EWSR1* gene to related members of the ETS family of transcription factors has been used as an auxiliary diagnostic tool to support the histopathologic diagnosis of Ewing sarcoma. The broad sequence homologies between the *FUS/TLS* and the *EWSR1* genes indicate that they are derived from a common ancestor (29); thus, FUS could be an alternative translocation partner in Ewing sarcoma. Indeed, cases with *FUS/ERG* with t(16;21) and *FUS/FEV* with t(2;16) variant translocations have been described (30, 31). Some additional cases have been identified and diagnosed as undifferentiated small round cell sarcoma; with the involvement of the *EWSR1* gene in combination with ETS family members or without canonical EWSR1 fusion (32). This increasing number of translocation variants complicates molecular diagnosis. Currently, for negative cases by a RT-PCR designed for the two most frequent translocation variants (EWSR1/FLI1 or EWSR1/ERG), the use of FISH probes around the *EWSR1* locus are considered as diagnostic tools. Based on the previously discussed findings, a FISH probe detecting *FUS* gene rearrangements could be considered. The diagnosis of SRCT with a Ewing-like phenotype without rearrangements of either *EWSR1* or *FUS* genes may further complicate the diagnosis (32).

Despite the fact that all cases identified by us were from patients older than 18 years of age at the time of diagnosis and that they showed atypical cellular features, the immunohistochemical staining ($CD99^+$, periodic acid-$Schiff^+$, $vimentin^+$, $BCL2^+$, $S100^-$, $CD45^-$, $keratin^-$, $desmin^-$, CD3), in combination with the rearrangement of the *EWSR1* locus, justify the diagnosis of variant Ewing sarcoma both at the genetic and histologic levels. One can expect that tumors with atypical immunohistochemical features such as keratin, desmin, or S100 positivity at extraosseous locations in older patients would not be considered to be EWS at all if additional molecular tests to detect EWSR1 rearrangements were not done.

Intriguingly, a highly recurrent amplification pattern was observed in all three studied cases, showing a complex rearrangement between chromosomes 20 and 22 with a 4-fold amplification of the 5′ *EWSR1* gene (exons 1-8) and 3′ *NFATc2* (exons 2-11) regions. This observed pattern is an unusual phenomenon for tumors involving *EWSR1* gene translocations and is reported for the first time. Amplification might be responsible for a gene dosage effect, indicating a potentially weaker transforming potential, but coamplification of adjacent genes cannot be excluded. Similarly, amplification of the *PAX7/FKHR* or *COL1A1/PDGFB* fusion genes have been reported in rhabdomyosarcoma and dermatofibrosarcoma protuberans, respectively (33, 34).

In our study, we not only show the existence of a novel EWS-specific translocation in four cases, but we also showed for the first time tumorigenic activation of NFATc2 by chimera formation. Because the *NFATc2* gene resides in the critical minimal region of amplification in several solid tumors such as breast, colon, and esophageal cancer, next to the role described here in Ewing sarcoma, involvement of this transcription factor as a driver in the development of other tumors with or without chimera formation could be predicted. A similar mechanism has recently been described for prostate cancer, involving the *TMPRSS2* and *ERG* gene (35) and other ETS family members (36).

Disclosure of Potential Conflicts of Interest

No potential conflicts of interest were disclosed.

References

1. Fletcher CDM, Unni KK, Mertens F. World Health Organization classification of tumours. Pathology and genetics of tumours of soft tissue and bone. Lyon: IARC Press; 2002.
2. Sandberg AA, Bridge JA. Updates on cytogenetics and molecular genetics of bone and soft tissue tumors: Ewing sarcoma and peripheral primitive neuroectodermal tumors. Cancer Genet Cytogenet 2000; 123:1–26.
3. Rossi S, Szuhai K, Ijszenga M, et al. EWSR1-1 and EWSR1-1 fusion genes in angiomatoid fibrous histiocytoma. Clin Cancer Res 2007;13:7322–8.
4. Mitelman F, Johansson B, Mertens F. Mitelman database of chromosome aberrations in cancer; 2008. Available from: http://cgap.nci.nih.gov/Chromosomes/Mitelman.
5. Moller E, Stenman G, Mandahl N, et al. POU5F1, encoding a key regulator of stem cell pluripotency, is fused to EWSR1 in hidradenoma of the skin and mucoepidermoid carcinoma of the salivary glands. J Pathol 2008;215:78–86.
6. Janknecht R. EWS-ETS oncoproteins: the linchpins of Ewing tumors. Gene 2005;363:1–14.
7. Bovee JVMG, Devilee P, Cornelisse CJ, Schuuring E, Hogendoorn PCW. Identification of an EWS-pseudogene using translocation detection by RT-PCR in Ewing's sarcoma. Biochem Biophys Res Commun 1995;213:1051–60.
8. Verger A, Duterque-Coquillaud M. When Ets transcription factors meet their partners. Bioessays 2002; 24:362–70.
9. Verger A, Buisine E, Carrere S, et al. Identification of amino acid residues in the ETS transcription factor Erg that mediate Erg-Jun/Fos-DNA ternary complex formation. J Biol Chem 2001;276:17181–9.
10. Kim S, Denny CT, Wisdom R. Cooperative DNA binding with AP-1 proteins is required for transformation by EWS-Ets fusion proteins. Mol Cell Biol 2006; 26:2467–78.

11. Braunreiter CL, Hancock JD, Coffin CM, Boucher KM, Lessnick SL. Expression of EWS-ETS fusions in NIH3T3 cells reveals significant differences to Ewing's sarcoma. Cell Cycle 2006;5:2753–9.

12. Hancock JD, Lessnick SL. A transcriptional profiling meta-analysis reveals a core EWS-FLI gene expression signature. Cell Cycle 2008;7:250–6.

13. Macian F, Lopez-Rodriguez C, Rao A. Partners in transcription: NFAT and AP-1. Oncogene 2001;20: 2476–89.

14. Macian F. NFAT proteins: key regulators of T-cell development and function. Nat Rev Immunol 2005;5: 472–84.

15. Szuhai K, Ijszenga M, Tanke HJ, et al. Detection and molecular cytogenetic characterization of a novel ring chromosome in a histological variant of Ewing sarcoma. Cancer Genet Cytogenet 2007;172:12–22.

16. Knijnenburg J, van der BM, Tanke HJ, Szuhai K. Optimized amplification and fluorescent labeling of small cell samples for genomic array-CGH. Cytometry A 2007;71:585–91.

17. Szuhai K, Bezrookove V, Wiegant J, et al. Simultaneous molecular karyotyping and mapping of viral DNA integration sites by 25-color COBRA-FISH. Genes Chromosomes Cancer 2000;28:92–7.

18. Wiegant J, Kalle W, Mullenders L, et al. High-resolution *in situ* hybridization using DNA halo preparations. Hum Mol Genet 1992;1:587–91.

19. Szuhai K, Ijszenga M, Tanke HJ, Rosenberg C, Hogendoorn PCW. Molecular cytogenetic characterization of four previously established and two newly established Ewing sarcoma cell lines. Cancer Genet Cytogenet 2006;166:173–9.

20. Hogan PG, Chen L, Nardone J, Rao A. Transcriptional regulation by calcium, calcineurin, and NFAT. Genes Dev 2003;17:2205–32.

21. Rao A, Luo C, Hogan PG. Transcription factors of the NFAT family: regulation and function. Annu Rev Immunol 1997;15:707–47.

22. Jin L, Sliz P, Chen L, et al. An asymmetric NFAT1 dimer on a pseudo-palindromic κB-like DNA site. Nat Struct Biol 2003;10:807–11.

23. Verhoeven DH, de Hooge AS, Mooiman EC, et al. NK cells recognize and lyse Ewing sarcoma cells through NKG2D and DNAM-1 receptor dependent pathways. Mol Immunol 2008;45:3917–25.

24. de Hooge AS, Berghuis D, Santos SJ, et al. Expression of cellular FLICE inhibitory protein, caspase-8, and protease inhibitor-9 in Ewing sarcoma and implications for susceptibility to cytotoxic pathways. Clin Cancer Res 2007;13:206–14.

25. Chen L, Glover JN, Hogan PG, Rao A, Harrison SC. Structure of the DNA-binding domains from NFAT, Fos and Jun bound specifically to DNA. Nature 1998; 392:42–8.

26. Ramirez-Carrozzi VR, Kerppola TK. Dynamics of Fos-Jun-NFAT1 complexes. Proc Natl Acad Sci U S A 2001;98:4893–8.

27. Marinescu VD, Kohane IS, Riva A. MAPPER: a search engine for the computational identification of putative transcription factor binding sites in multiple genomes. BMC Bioinformatics 2005;6:79.

28. Hollenhorst PC, Jones DA, Graves BJ. Expression profiles frame the promoter specificity dilemma of the ETS family of transcription factors. Nucleic Acids Res 2004;32:5693–702.

29. Aman P, Panagopoulos I, Lassen C, et al. Expression patterns of the human sarcoma-associated genes FUS and EWS and the genomic structure of FUS. Genomics 1996;37:1–8.

30. Ng TL, O'Sullivan MJ, Pallen CJ, et al. Ewing sarcoma with novel translocation t(2;16) producing an in-frame fusion of FUS and FEV. J Mol Diagn 2007;9: 459–63.

31. Shing DC, McMullan DJ, Roberts P, et al. FUS/ERG gene fusions in Ewing's tumors. Cancer Res 2003;63: 4568–76.

32. Wang L, Bhargava R, Zheng T, et al. Undifferentiated small round cell sarcomas with rare EWS gene fusions: identification of a novel EWS-SP3 fusion and of additional cases with the EWS-ETV1 and EWS-FEV fusions. J Mol Diagn 2007;9:498–509.

33. Davis RJ, Barr FG. Fusion genes resulting from alternative chromosomal translocations are overexpressed by gene-specific mechanisms in alveolar rhabdomyosarcoma. Proc Natl Acad Sci U S A 1997; 94:8047–51.

34. Sandberg AA, Bridge JA. Updates on the cytogenetics and molecular genetics of bone and soft tissue tumors. Dermatofibrosarcoma protuberans and giant cell fibroblastoma. Cancer Genet Cytogenet 2003; 140:1–12.

35. Tomlins SA, Rhodes DR, Perner S, et al. Recurrent fusion of TMPRSS2 and ETS transcription factor genes in prostate cancer. Science 2005;310:644–8.

36. Tomlins SA, Laxman B, Dhanasekaran SM, et al. Distinct classes of chromosomal rearrangements create oncogenic ETS gene fusions in prostate cancer. Nature 2007;448:595–9.